Seismic constraints on the three-dimensional geometry of low-angle intracrustal reflectors in the Southern Iberia Abyssal Plain

S. M. Dean, T. A. Minshull and R. B. Whitmarsh
National Oceanography Centre, Southampton SO14 3ZH, UK.
E-mail: smd9@noc.soton.ac.uk

Accepted:

Received:

In original form:

Abbreviated title: Low-angle reflectors on the west Iberia margin

Corresponding author:

Simon Dean,
National Oceanography Centre, Southampton,
European Way,
Southampton SO14 3ZH
U.K.

E-mail: smd9@noc.soton.ac.uk
Tel: +44 (0)23 8059 2260
Fax: +44 (0)23 8059 3052

SUMMARY

Several lines of evidence suggest that simple shear rifting of the continental crust, in the form of low-angle detachment faulting, occurred during the final stages of continental breakup between West Iberia and the Grand Banks. The primary evidence for such faulting is the occurrence of low-angle, high amplitude reflectors within the basement adjacent to the ocean-continent transition zone. Here we present a series of intersecting, depth migrated seismic reflection profiles that image one such reflector, the H-reflector, located on the southern edge of Galicia Bank. 'H' lies beneath several boreholes drilled during ODP Legs 149 and 173, in a region where the oceanward extent of extended continental crust steps at least 150 km westward from its location in the southern Iberia Abyssal Plain to its location off the relatively shallow Galicia Bank. In our profiles 'H' appears to define a surface that extends over a region of at least 200 km^2 and that dips down ~19° to the north, towards Galicia Bank. The profiles show that a close affinity exists between 'H' and the most seaward continental crust. Based on geophysical data and ODP drilling results, we infer that the basement above 'H' is composed of continental crust deformed by extensional faults into a series of wedge-shaped blocks and thin slivers. These basement wedges have a complex three-dimensional geometry. 'H' rises to the basement surface on a number of the seismic profiles and appears to define locally the oceanward extent of continental fault blocks.

KEYWORDS

Continental margins; Controlled-source seismology; Crustal deformation; Faulting; Reflection seismology; Rifted margin.

1 INTRODUCTION

Rifted continental margins are formed when the continental lithosphere is progressively extended until either new oceanic crust is formed or the underlying mantle is exhumed to the seafloor (e.g., Whitmarsh *et al*. 2001). Over the past decade, observations of ancient rifted margins, both offshore and where they are exposed onshore by orogenic events subsequent to rifting, have led to new models in which extension along low-angle detachments plays a key role during the final stages of rifting (e.g., Manatschal 2004; Lavier & Manatschal 2006). However, to date these models have been primarily two-dimensional in nature. Here we present evidence that such detachments may have a complex three-dimensional geometry and that motion along them may not be confined to the overall extension direction of the margin. However, we do not attempt a rigorous structural interpretation of this geometry, which is beyond the scope of this paper.

Magma-poor rifted margins (sometimes termed "non-volcanic") offer the best opportunity to investigate the structures extruded by high degrees of continental extension since they are not obscured by subsequent magmatism and they do not undergo uplift and sub-aerial erosion. Many such margins have been identified: for example, Galicia Bank (Sibuet *et al*. 1987), the northern Bay of Biscay (Le Pichon & Barbier 1987), the Grand Banks (Keen *et al*. 1987), Southwest Greenland (Chalmers 1991), Northern Red Sea (Cochran & Martinez 1988) and Woodlark Basin (Benes *et al*. 1994). On multichannel seismic (MCS) reflection profiles acquired across magma-poor rifted margins the thinnest continental crust is typically characterized by rotated blocks of faulted continental crust. Faulting accommodates extension in the continental crust and most of the normal faults that bound crustal blocks dip down toward the centre of extension. In some cases these faults appear to flatten at depth and even merge onto a

single reflection event, frequently interpreted to be a detachment. It has been debated whether such detachments could be active at a low-angle (<30°), or were instead formed at a higher angle and rotated to a low-angle during subsequent extension (e.g., Buck 1988). However, there are documented examples of active low-angle extension in the Woodlark Basin (Abers *et al.* 1997) and the Gulf of Corinth (Reitbrock *et al.* 1996). An active low-angle detachment may coincide with a zone of mechanical weakness either within the continental crust, such as the brittle-ductile transition, or at the crust-mantle boundary. Similar low-angle features have been identified in continental rift areas such as the Basin and Range province in the western United States (e.g., Wernicke 1981; Lister & Davis 1989) and more recently have been inferred at inside corners of transform faults on mid-ocean ridges (e.g., Tucholke & Lin 1994; Ranero & Reston 1999).

The West Iberia margin is relatively sediment starved and is one of the most extensively studied magma-poor margins. Based on magnetic anomalies, the opening of the North Atlantic between Iberia and the Grand Banks region is inferred to have propagated from south to north. Seafloor spreading initiated in the Tagus Abyssal Plain at 133 Ma (M11; Whitmarsh & Miles 1995), in the southern IAP at ~128 Ma (M5, or just after; Russell & Whitmarsh 2003) and, west of Galicia Bank, some time after 120 Ma, during the Cretaceous Magnetic Quiet Interval (Ogg 1988; Pinheiro *et al*. 1996). The margin is segmented to form a series of bathymetric highs and lows: from south to north these are Gorringe Ridge, Tagus Abyssal Plain, Estremadura Spur, southern Iberia Abyssal Plain (IAP) and Galicia Bank (Fig. 1). The causes of the observed segmentation are poorly understood and this study looks at the three-dimensional structure of the basement and intrabasement reflectors at the boundary of two of these segments.

Our study area lies between the southern Iberia Abyssal Plain (IAP) and Galicia Bank, and encompasses several Ocean Drilling Program (ODP) Sites from Leg 149 and 173 (Fig. 1, inset). This region contains a number of characteristic basement features that are indicative of the underlying composition of the crust. The Peridotite Ridge (PR) is an enigmatic basement feature identified as a series of four, apparently overlapping, segments that run approximately north-south between ~12–13°W along the northern half of the West Iberia margin (Beslier *et al*. 1993; Pickup *et al*. 1996; Henning *et al*. 2004). More detailed analysis suggests that these segments themselves may be also discontinuous (Péron-Pinvidic *et al.* 2008). The PR has been sampled west of Galicia Bank by dredging, from submersible and by ODP Leg 103, and in our study area by ODP Legs 149 and 173. West of the PR unambiguous seafloor-spreading magnetic anomalies are identified (Whitmarsh & Miles 1995; Russell & Whitmarsh 2003) including the J-magnetic anomaly (Pinheiro *et al*. 1992) and the seismic velocity structure of the basement lies within the bounds of normal Atlantic oceanic crust (Dean *et al.* 2000); therefore the oceanward limit of the PR approximately coincides with the landward extent of unambiguous oceanic crust, as defined by geophysical measurements. The oceanward extent of extended continental crust is defined by rotated basement blocks and wedges, identified on seismic reflection profiles and sampled by ODP drilling.

Extended continental crust on this part of the margin is associated with a pair of strong sub-basement reflectors: the S-reflector (de Charpal *et al*. 1978) west of Galicia Bank and the H-reflector (Krawczyk *et al*. 1996) in our study area. The H- and S-reflectors strongly resemble one another and are both interpreted to be closely associated with the final stages of rifting (e.g., Boillot *et al*. 1988; Krawczyk *et al*. 1996; Whitmarsh *et al*.

2001; Manatschal 2004). In the southern IAP, south of our study area, the most oceanward continental crust is identified on profile IAM-9 at ~10°45'W (Pickup *et al*. 1996; Dean *et al*. 2000); west of Galicia Bank wedges of continental crust are identified significantly further west, to nearly 13°W and within 15 km of the PR (e.g., Reston *et al.* 1996). Therefore the distance between the oceanward extent of continental crust and the PR dramatically reduces northward along the margin. The PR and the region between the PR and continental crust is variously referred to as the ocean-continent transition zone (OCT), transition zone (TZ, excluding the PR; Pickup *et al*. 1996), or zone of exhumed continental mantle (ZECM; Whitmarsh *et al*. 2001). The basement in this region is interpreted to be composed of exhumed and partially serpentinized mantle peridotite. This zone also appears in reconstructions of the North Atlantic along the M0 isochron (e.g., Srivastava & Verhoef 1992), which fit the southern IAP with the southern edge of Flemish Cap. Such reconstructions close the Atlantic between the conjugate Galicia Bank and Flemish Cap margins, but leave a significant gap in the southern IAP. The gross rifting structures in this region, determined from published MCS reflection profiles, are summarized by three E-W oriented time-section profiles that span the full ocean-continent transition zone: IAM-11 to the north of our study area, IAM-9 to the south, and Lusigal 12 in our study area (Fig. 2).

IAM-11 (Fig. 2A) is located over Galicia Bank, and shows a similar structure to numerous adjacent profiles including GP101 (Reston *et al.* 1996). A series of rotated blocks of continental crust are bounded by faults that appear to merge downwards onto the S-reflector, a single low-angle reflection event, roughly flat in a depth-migrated section (Reston *et al*. 1996) but appearing sinuous in a time section. Oceanward, the S-reflector either rises to the basement (Boillot *et al.* 1988) or is truncated against the

landward side of the PR. Toward the continent, the S-reflector rises to the basement to form a clear breakaway and, although further fault-bounded blocks of continental crust are identified, all the associated bounding faults have a relatively high angle.

IAM-9 (Fig. 2C) lies in the southern IAP and shows a markedly different structure from IAM-11 further north. A 130-km-wide region of generally low basement relief is interpreted to be composed of serpentinized mantle peridotite, exhumed after continental break-up and prior to onset of seafloor spreading. Based on wide-angle seismic and surface and deep-towed magnetic data, this region is interpreted to contain little or no decompression melt products (e.g., Dean *et al*. 2000; Russell & Whitmarsh 2003). Although landward of this region faulted blocks of continental crust are identified, they are not associated with any low-angle reflectors in this profile (Pickup *et al*. 1996). A discontinuous Moho reflection is observed beneath the continental blocks but no Moho reflection is observed in the zone of exhumed mantle. On the oceanward side of this zone, the PR appears much wider compared to west of Galicia Bank, due in part to the overlap of segments R3 and R4 (Fig. 1). The continental flank of the PR is clearly defined by a pair of high-angle landward dipping reflectors, L1 and L2. Reflector L1 bounds PR segment R4 (Pickup *et al*. 1996) but the landward extent of the PR, based on seismic velocity, is defined by L2 (Dean *et al*. 2000).

The Lusigal 12 profile shares common features with IAM-11 and IAM-9 and has the advantage of basement sampling on, or close to, the profile at six ODP Sites from Legs 149 and 173 (Fig. 2B). Pre-rift sediment has been sampled at Sites 901 and 1065 (ODP Leg 173 Shipboard Scientific Party 1998) on top of fault bounded blocks of continental crust, identified at the east end of the profile. Oceanward of Site 1065 the H-reflector is observed (Krawczyk *et al*. 1996). The H-reflector is a high amplitude reflection event

onto which the faults bounding the basement blocks located between Site 1065 and the basement high known as the 'Hobby High' that was drilled at Site 900, 1067 and 1068, appear to flatten and merge. Krawczyk *et al*. (1996) interpret the H-reflector to form a 15–20 km wide 'U' shaped synrift detachment fault that reaches a maximum depth of ~9.5 km and intersects the basement surface just oceanward of Site 1065 and again on the Hobby High. Later interpretations have refined a number of details including a high angle fault in the toe of the continental wedge that rises at the Hobby High (Whitmarsh *et al*. 2000). In the most recent models for the evolution of this part of the margin the H-reflector is interpreted as one of several detachment faults that cut right through the crust and into the mantle, and that have rotated to very low angle during the final stages of rifting (e.g., Whitmarsh *et al*. 2001; Manatschal 2004). The samples recovered from the Hobby High are most likely from the lower continental crust (Whitmarsh *et al.* 2000), which supports the seismic interpretation that Site 900 sampled the toe end of a wedge-shaped faulted block of continental crust. The PR is identified at the oceanward end of Lusigal 12, but lies ~75 km from Site 900. Unlike on IAM-9, the basement between the PR and the continental blocks east of the Hobby High has significant topography. However, wide-angle seismic data show a similar velocity structure to that found on IAM-9 (Chian *et al.* 1999). The basement high beneath Site 898 appears to be the extension of R4 (Fig. 1, inset) and is bounded by a landward dipping reflector similar to L2. Site 1069, situated on a basement high north of Lusigal 12, recovered sediments analogous to those at Site 901 and 1065 and is interpreted as a continental allochthon (e.g., Manatschal *et al.* 2001).

In summary, while the most oceanward continental crust and the Peridotite Ridge have a very similar appearance along the margin, there is a dramatic variation in the width of

the region between them from 130 km in the southern IAP to almost zero at Galicia Bank. Similarly the location of the most oceanward continental crust steps approximately 150 km further west in less than 200 km distance along margin. Our study area, the Lusigal 12 profile and the ODP drilling transect, are located close to these changes.

2 ACQUISITION AND PROCESSING OF REFLECTION DATA

Seismic reflection profiles CAM 144, CAM 146, CAM 159 and CAM 160 were acquired during August 1995 as part of an experiment involving coincident ocean-bottom seismic (OBS) wide-angle seismic profiles (Discovery 215 Working Group 1998; Chian *et al*. 1999). The seismic source used was a 6346 cu. in. (~104 litres) 12-airgun array. The source was tuned with a peak frequency response of between 8 and 10 Hz to provide both strong, long offset, energy to the OBS receivers and deep normal-incidence penetration beneath the basement. In the MCS data, clear sub-basement primary reflections are identified as deep as the seafloor multiple (~14 s two-way time) on some profiles. The sedimentary architecture of the margin, based on these and other profiles, is described by Péron-Pinvidic *et al*. (2007), while the expression of post-rift compressional tectonics and its relationship to basement composition is described by Péron-Pinvidic *et al*. (2008). These studies were focused on time sections, rather than depth sections, and do not address the geometry of sub-basement reflectors.

The initial processing scheme, applied to the unstacked MCS data, is given in Table 1. Data were resampled from 4 ms to 8 ms and adjusted for amplitude using time-squared gain recovery. Predictive deconvolution was applied using a 200 ms operator with an 80 ms gap length to remove short period sediment multiples, followed by a bandpass

filter with a pass range of 5–20 Hz. The 48-channel streamer employed, with a group interval of 50 m, gives source-receiver offsets from 207 m to 2557 m. The source was triggered every 50 s, which equates to a distance of ~125 m and gives an average fold of 9–10. After depth migration a 20 m static correction was applied to account for the depth of the source and receivers below the sea surface.

The main objectives of our processing scheme were to provide both a clear and a geometrically accurate image of the sub-basement reflectors. These objectives were achieved using prestack depth migration. Depth migration has a significant advantage over, for example, a conventional time migration followed by depth conversion, because it corrects for distortion in the input time domain seismic data caused by lateral velocity variations (e.g., Judson *et al*. 1980; Yilmaz 1987). Lateral velocity variations are significant on the West Iberia margin largely due to the rugged basement relief (e.g., Reston *et al*. 1996; Krawczyk *et al*. 1996). Migration of prestack data has the advantage of removing diffractive events more successfully since they have not been stacked into the seismic section as noise.

3 DETERMINING MIGRATION VELOCITY MODELS

We use depth focusing error migration velocity analysis (Jeannot *et al*. 1986) to determine optimal migration velocity models for profiles CAM 144, CAM 146 and CAM 160. Focusing analysis has been used with excellent results to analyse and depth migrate MCS data acquired on the West Iberia margin by Hoffmann & Reston (1992), Reston *et al*. (1996) and Pickup *et al*. (1996). The velocity model for each MCS profile was constructed using a series of layers, each of which was defined to follow a significant reflector that can be identified and traced laterally across profile

intersections. A significant reflector is one that provides clear velocity analyses at as many analysis locations as possible. Since focusing analysis performed on any reflector is dependent on the velocity of the overburden, to achieve a rapid convergence to the optimum velocity model the shallow velocity structure was determined first. Starting with a migration at the water velocity, the velocity model was constructed in an iterative scheme, alternating between depth migration and velocity analysis to analyse successively deeper layers. Up to seven iterations of focusing analysis were performed on each MCS section before reaching the final migrated image. At intersections between profiles, the velocity of each model layer was compared and adjusted so that all the models match. CAM 159 was processed later, without focusing analysis, but with a migration velocity model that ties at the intersections with CAM 144 and CAM 146 and thus provides a consistent result. The final migration velocity models are presented in Figs 3A–6A.

In the final velocity models seven constant velocity layers represent the post-rift sedimentary sequence. The layers vary in velocity between 1.7 km s^{-1} at the seafloor up to a maximum of 3.5 km s^{-1} where the basement is deepest. An eighth layer, interpreted to represent synrift and/or post-rift sediment in a number of locations, has a velocity of 3.8 km s^{-1}. The velocity within the basement could not be satisfactorily determined using our MCS data because individual focusing analyses on intra-basement reflectors were poorly constrained and, where the reflectors are laterally continuous, adjacent analyses were often inconsistent. We attribute the poor analyses to both the reduced range of incidence angles sampled at basement depths of >6 km, and to the dipping structure and lateral velocity variations, caused by the complex basement topography, that reduce the effectiveness of the analysis technique (MacKay & Abma 1992). In

addition, the geometry of the sub-basement reflectors requires a complex structural interpretation if they are to be modelled as a series of velocity layers; such a highly developed interpretation is undesirable at this stage in the analysis since it risks introducing migration artefacts, particularly at the boundaries between velocity layers, that could then be mistakenly interpreted as real structure. Our solution is to extend, in depth, the sediment velocity model derived from focusing analysis using the basement velocity structure derived from wide-angle seismic data (Discovery 125 Working Group 1998; Chian *et al*. 1999; Dean *et al*. 2000). Wide-angle seismic data provide an ideal smooth velocity model for depth migration below the basement since such data constrain mainly long-wavelength velocity variations and are most sensitive to vertical changes in velocity, important in the southern IAP where a Moho reflection is not generally observed.

Chian *et al*. (1999) presented a series of wide-angle seismic profiles in the vicinity of, and including, CAM 144 and the Hobby High. The basement velocity varies between ~5.3 km s^{-1}, on CAM 144 ~10 km north of the Hobby High, and ~4.2 km s^{-1}, on CAM 142 ~10 km south of the Hobby High. The lateral decrease in basement velocity was interpreted to coincide with a change in the composition of the basement from extended continental crust to serpentinized peridotite. Below basement, the velocity increases to ~7.7 km s^{-1} at ~12 km depth in both CAM 142 and CAM 144. They modelled a velocity step of ~0.7 km s^{-1} at ~10 km depth, which coincides with the H-reflector on CAM 144, but does not match any reflection event on CAM 142. Since a coincident wide-angle velocity model is only available for CAM 144, we chose to simplify Chian *et al.*'s basement velocity structure to a single layer with a linearly increasing velocity from ~4.5 km s^{-1} at the basement to 8 km s^{-1} at a constant depth of

12 km for all sections. This velocity structure is compatible with other wide-angle models for the basement in the southern IAP (Discovery 125 Working Group 1998; Dean *et al*. 2000). At very shallow basement highs the velocity at the basement is reduced to 4.2 km s^{-1}, which ensures that the velocity step at the basement does not exceed 1 km s^{-1}. Below 12 km depth the velocity is a constant 8 km s^{-1}. The strength of reflection events beneath the basement after migration are not very sensitive to the migration velocity; our velocity model has the advantage of being consistent between sections and minimizes velocity steps, particularly at the basement, which could cause artefacts in the migrated sections.

4 UNCERTAINTY IN THE MIGRATION VELOCITY MODELS

By defining our sediment velocity models as a series of constant velocity layers, we introduce first-order discontinuities of up to 1 km s^{-1} between model layers. Such large velocity steps are unlikely to be geologically realistic within the sediments or even across the sediment-basement transition. Although seismic velocity will, on the large scale of this survey, generally increase smoothly with increasing depth, it is not possible to constrain a vertical velocity gradient within model layers with the analysis technique we employed where the thicknesses of the model layers do not significantly change laterally. Except for the sediment layers that lie within the basement lows, most of our sediment velocity layers have a near constant thickness across each section. In addition, Versteeg (1993) shows that it is the long wavelength variations in the velocity model that most strongly influence the migrated image, even for a very complicated structure. Therefore, our migrated sections are unlikely to be improved using a more complicated velocity model.

Although the implementation of depth focusing analysis we employ does not provide for any direct statistical analysis of the uncertainty in the migration velocity model, this uncertainty can be estimated from the uncertainty in picking the depth focusing error. In the depth focusing panels (Jeannot *et al*. 1986), the width of the amplitude maxima for each reflector is related to how well the energy is focused at migration velocities slightly higher and lower than the optimum velocity. We estimate the uncertainty in the mean interval velocity for each model layer by dividing the uncertainty in picking the depth focusing error by the two-way travel-time through the layer; this function is shown graphically in Fig. 7. Velocity uncertainty is greatest for a thin, high velocity layer and generally increases with depth where migrated energy is less sharply focused at the optimum migration velocity. Given that the velocity layers, defined in our models, range in thickness between 0.2 s and 0.5 s two-way time, for an estimated uncertainty of 0.04 km in picking the depth error, the uncertainty in each migration velocity analysis is between 0.17 km s^{-1} and 0.4 km s^{-1}. Since each model velocity layer was determined from the average of a number of velocity analyses spread along the section, and sediment velocities in this region vary little laterally (e.g., Chian *et al.* 1999; Dean *et al.* 2000), the velocity uncertainty for each model layer estimated in Fig. 7 is likely to be an upper bound.

5 DEPTH MIGRATED SECTIONS

5.1 Sedimentary Units

The final migrated sections are presented in Figs 3B–6B. The total sediment thickness varies between ~0.5 km and 4 km. The post-rift sedimentary succession is identified as

sub-horizontal reflectors that onlap, or slightly drape, the basement highs. The seismic reflectors used to define the model layers coincide with some of the post-rift sedimentary Units 1–6 identified by Wilson *et al*. (1996) around the ODP Leg 149 drill sites; the approximate velocity of each sedimentary unit is given in Table 2.

Although the primary purpose of this work is to understand the sub-basement structure, a curious feature is apparent in our data at the top of sediment Unit 6 which has not been noted before. Adjacent to the basement high on CAM 146 east of CDP 1540 and on CAM 144 symmetrically between basement highs at CDP 1300 and CDP 2450, the reflection from the top of Unit 6 significantly increases in amplitude. The origin of the anomalous amplitudes is not clear from the data. One possibility is that a high velocity layer in the sediment causes them. On CAM 144 a vertical offset is observed in the underlying sediment and basement reflections in both the time and depth migrated data (Fig. 8A). The offset could be related to movement along a fault plane, but also lies directly beneath the edge of one of the high amplitude regions, above which the offsets in reflectors stop. The introduction of a relatively high (4.1 km s^{-1}) velocity layer into the migration velocity model, at the top of sediment Unit 6, reduces the offsets in the underlying sediment reflectors (Fig. 8C). However, the basement reflection is less sharply imaged with the high velocity layer and it is not included in the final migration velocity model.

Synrift sediments occur in basement lows as wedge shaped units with a weakly layered internal seismic structure comprised of reflectors that fan out as the layer thickens, typical of a sedimentary unit that was deposited onto a growth fault while extension was taking place (Péron-Pinvidic *et al*. 2007). They are identified in all of the sections, but particularly clear examples are observed on CAM 144 between CDP 1400 and 1700,

and between CDP 2100 and 2300 (Fig. 4). The synrift units are very similar in appearance to those identified by Krawczyk *et al*. (1996) on Lusigal 12.

5.2 Sub-basement reflections

The H-reflector is identified in the profiles through ties to its expression in the Lusigal 12 profile (Krawczyk *et al*. 1996). It should be noted that, in general, after migrating intersecting two-dimensional seismic sections across a structure with significant dip the reflectors are not expected to tie exactly since each migration images a different apparent dip and the reflection event should move in or out of the plane of each section to a certain degree. A three-dimensional migration would not have this problem but our data are not suitable for such processing. The process of tying the H-reflector between intersecting profiles is most reliably performed using unmigrated stacked sections, which provide a close approximation to zero-offset sections and avoid mis-ties because at the point of intersection: (1) a dipping reflector will appear at the same travel-time on both sections; (2) time-sections avoid any possible depth error due to an inconsistency in the velocity model used to migrate each profile. The H-reflector is readily identified in unmigrated stacked sections as a discrete reflection event with significantly higher amplitude compared to the generally low sub-basement reflectivity (e.g., Fig. 2B) and is successfully tied between all the presented CAM profiles (Fig. 9). The process of depth migrating the CAM profiles does not remove the discrete, relatively high-amplitude characteristic of the H-reflector. Depth migrating the CAM profiles removes the strong diffractions originating from the rough basement topography, improving the lateral continuity of the H-reflector and hence aids its identification. At the intersection between profiles the H-reflector can be tied successfully in depth; we attribute this to

the relatively low dip of the H-reflector and that the method used to create the migration velocity models ensures that the velocity structure matches at the intersection between each profile. On CAM 144, CAM 146 and Lusigal 12 a series of sub-basement reflectors dipping down to the west can be traced as continuous events from the basement down to the H-reflector. The westward dipping reflectors are associated with offsets in the basement and separate the basement into a series of roughly wedge shaped blocks. We now consider the sub-basement reflections on each profile in detail.

5.3 CAM 146

CAM 146 (Fig. 3) lies ~5 km south of and parallel to Lusigal 12 and appears to image a very similar structure. An H-like reflector is identified across ~20 km of the section as a near linear event dipping at a low angle (<5°) down to the west between CDP 1500 and CDP 2250, the eastern flank of the southward continuation of the Hobby High. East of CDP 1500 this reflector becomes poorly imaged due to edge effects in the depth migration. It is not possible to distinguish whether the H-reflector intersects the basement at CDP 1500 or whether it continues east, beneath the basement, and out of the section (dashed line; Fig. 3C). While it is tempting to interpret the entire event to be the H-reflector, after tying this profile to CAM 160 (Fig. 10) and Lusigal 12 it becomes apparent that the H-reflector must rise to the basement at CDP 1850. The Hobby High forms a generally rounded basement feature that is characterized by a small peak in the topography on its eastern side. From the eastern side of the small peak a steeply eastward dipping (~50°) reflector is identified down to 12.5 km depth and either merges with, or truncates, the H-reflector. From the western side of the small peak a westward dipping (~22°) reflector is observed to ~8.5 km depth that appears to mark a boundary

in the reflective character of the upper 2–3 km of the basement. Above the westward dipping reflector the sub-basement contains many reflectors without any coherent structure. Below the westward dipping reflector no strong reflectors are observed. Between CDP 1650 and 2050 a westward dipping reflector is observed, similar in amplitude to the H-reflector, but with a steeper dip (~18°) and imaged to a greater depth (dashed line; Fig. 3C). The deeper reflector can be tied to a similar event on CAM 160 (Fig. 10) and may be the continuation of one of the faults bounding a basement block.

5.4 CAM 144

CAM 144 (Fig. 4) lies ~10 km north of Lusigal 12, 15 km north of CAM 146, and is approximately parallel to both. The H-reflector is identified but poorly imaged at ~11.5 km depth beneath CDP 2375, the intersection with CAM 160. The H-reflector appears to shoal west of CDP 2375 but cannot be traced as a laterally continuous reflection event. The basement high beneath CDP 1950 is the northward continuation of the Hobby High and has a more rounded shape compared to the next basement high to the east. Beneath the northward continuation of the Hobby High, three reflectors, each ~2.5 km long with a very shallow dip down to the west, appear to form a series of steps up to the west. The offset between each reflector is approximately 0.5 km and the three reflectors appear to have very little, if any, overlap. The three reflectors can be interpreted either as a set of low-angle westward dipping normal faults (Fig. 4C) or as a single reflector which has been offset by a set of high-angle eastward dipping faults (Fig. 4D). The strongest sub-basement reflection events on CAM 144 are a pair of westward dipping (~22°) reflectors that can be traced from the basement at CDP 1600 and CDP 2300, beneath the deep basement lows filled with wedge shaped sedimentary

units. The eastern strong sub-basement reflector lies above the H-reflector near to the intersections with CAM 159 and CAM 160, and may merge with the H-reflector further west, although this is not imaged. The western strong sub-basement reflector may merge with the shallowest of the reflectors that form the steps beneath the central basement high (Fig. 4D); it can be traced close to the western edge of the section at a maximum depth of 10.5 km, where it appears to be offset by ~0.5 km, possibly by a steeply eastward dipping reflector (c.f., the H-reflector east of the Hobby High on CAM 146 and Lusigal 12). The westward dipping reflectors are interpreted to represent fault planes bounding large basement blocks.

5.5 CAM 159

The H-reflector is not clearly imaged anywhere on CAM 159 (Fig. 5). At the northeast end of the section a weak reflection is detected at ~10.5 km depth which ties to the H-reflector identified on CAM 144. Between CDP 800 and 1250 a sub-basement reflection is well imaged but must lie above the H-reflector since it ties with the eastern of the two strong westward dipping reflectors on CAM 144 and lies between two basement blocks. At the intersection with Lusigal 12, the strong sub-basement reflector on CAM 159 ties with the H-reflector (Krawczyk *et al*. 1996). The H-reflector on CAM 159 must dip up to the southwest from the intersection with CAM 144 and merge with the strong sub-basement reflector (Fig. 5C). Two possible interpretations for the H-reflector are given; because the H-reflector is observed as a linear event that only dips down to the north on CAM 160 (Fig. 6C), our favoured interpretation for CAM 159 is that the H-reflector follows the shallower, less steeply dipping, of the reflectors. The strong sub-basement reflector intersects the basement close to CDP 800, north of the intersection with

CAM 146. There is a weak indication of a reflector that dips down to the northeast at a very steep angle and may either cross or truncate the H-reflector. The steep dipping reflector on CAM 159 is similar to the steep eastward dipping reflector on the eastern flank of the Hobby High identified on CAM 146. Although it is not clear from the data, in Fig. 5C the steep dipping event is interpreted to offset the H-reflector in accord with the interpretation of Lusigal 12 (Manatschal 2004).

5.6 CAM 160

On CAM 160 (Fig. 6) the H-reflector dips down at ~20° to the north, toward Galicia Bank, from CDP 600 and reaches a maximum depth of ~11.5 km before it becomes too weak to identify, probably as a result of edge effects in the migration. From the basement at CDP 1000 a strong reflector dips down to the north at ~7° and merges with the H-reflector at CDP 400. This reflector appears almost identical in character to the H-reflector and, similar to the reflector on CAM 146, until the reflection is tied to Lusigal 12 it is tempting to interpret it as the H-reflector. Above this reflector the basement is divided into two, possibly three, wedge shaped blocks, which have the same well-defined basement reflection and weak internal reflective character as the basement blocks above the H-reflector. At the intersection with CAM 146 (Fig. 10) the blocks on CAM 160 are identified to be overlain by the synrift sediment units identified earlier and the reflectors bounding the wedge shaped blocks tie with the westward dipping reflectors on CAM 146.

6 DISCUSSION

Combining the interpretations of the four CAM profiles presented in this paper and of Lusigal 12 provides a three-dimensional view of the basement in the vicinity of the Hobby High (Fig. 11). To be consistent with existing interpretations of Lusigal 12 (e.g., Manatschal 2004), the H-reflector rises to the basement on the western flank of the Site 1065 basement high on Lusigal 12 and CAM 144.

Tracing the H-reflector south on CAM 160 from the intersection with Lusigal 12 and east on CAM 146, i.e., in the south-eastern part of the study area, several distinct interpretations are possible: a) the H-reflector immediately rises to the basement close to the intersection between CAM 160 and CAM 146 with the 'H' breakaway at CDP 600 on CAM 160 and at CDP 1825 on CAM 146 (Fig. 11, main image); b) the H-reflector continues further southeast, rising to the basement with the 'H' breakaway either at CDP 850 or at CDP 1000 on CAM 160, and somewhere east of CDP 1600 on CAM 146 (Fig. 11, inset).

In the first, our favoured, scenario (Fig. 11, main image) the H-reflector forms a simple curving structure that cuts down from the basement at a point progressively further west from north to south (CAM 144 to CAM 146) and forms a surface that extends laterally over an area of at least 200 km^2. The other low-angle faults identified on CAM 146 and CAM 160 lie beneath the H-reflector and represent at least two fault surfaces that curve to the southwest in a similar pattern to the H-reflector. On CAM 144 the low-angle faults join with the west-dipping faults identified beneath the Site 1065 basement high. Since the basement wedges identified on CAM 146 below the H-reflector have a very similar appearance to the basement wedges above the H-reflector they are interpreted to have formed on the same detachment surface, i.e., the H-reflector has the same

structural significance as the other west-dipping faults, and they all sole onto a common detachment surface. This interpretation is similar to the alternative presented by Krawczyk *et al.* (1996; their Fig. 10C) and suggests that the detachment extends further to the east than in many previous interpretations based on the Lusigal 12 profile alone (e.g., Whitmarsh *et al.* 2000; Whitmarsh *et al.* 2001; Manatschal *et al.* 2001; Manatshal 2004). If the detachment identified on CAM 144 and CAM 146 extends beneath the faulted blocks of continental crust to at least the east end of each profile, and on CAM 160 as far south as CDP 1000, it would represent slip over an area in excess of 600 km^2.

In the second, alternative scenario, extending the H-reflector beneath the basement to the south and east (Fig. 11, inset) would place the breakaway further east on CAM 146 than on Lusigal 12 and CAM 144. This scenario would require the wedges identified on CAM 160 between CDP 600 and CDP 1000 to represent very thin slivers of crust no more than 1–1.5 km thick extending over an area at least 10 km wide. The faults that bound these slivers are inferred to merge with or truncate against the H-reflector south of Lusigal 12 since they are not identified on this profile. There is no strong evidence for such slivers elsewhere in our data: although one interpretation for CAM 144 cuts the crust into a number of thin slivers (Fig. 4C), this interpretation is not consistent with the high-angle fault adjacent to Hobby High; the apparent sliver drilled at Site 1069 turns out to be the toe end of a basement wedge that thickens significantly to the north when viewed on other profiles. In the first scenario the thin basement on CAM 160 represents the southern tip of wedges that thicken to the north.

Our data show that there are significant margin-parallel changes in the structure of the continental crust in this part of the west Iberia margin. For example, the Hobby High forms one of a sequence of elongate basement highs in the southern IAP (Discovery 215

Working Group 1998; Péron-Pinvidic *et al.* 2007), and on CAM 144, the northern-most profile, is formed of a faulted continental block, but on Lusigal 12, only ~10 km south, the continental crust is very much thinner and on CAM 146, a further ~5 km south, has disappeared altogether. Therefore the basement highs only superficially represent a simple margin-parallel structure. In general, the wedges of continental crust that are characteristic of the east-west seismic profiles taper out to the south on the southern edge of Galicia Bank. The wedge lying above the eastern end of the H-reflector on Lusigal 12 shows this most clearly, becoming thicker to the north on CAM 144 and thinner to the south on CAM 146. This observation is significant for the interpretation of the block drilled at Site 1069 (Manatschal 2004), which is likely to be the southern tip of a tapering basement wedge that forms the basement high (Fig. 12), and is therefore a part of the crust of Galicia Bank, rather than an isolated continental block.

The high-angle fault adjacent to the Hobby High, identified by Whitmarsh *et al.* (2000), appears on CAM 146, CAM 159 and Lusigal 12, and forms a roughly northwest-southeast trending normal fault dipping down to the northeast. This fault offsets the H-reflector and must therefore post-date it. Our preferred interpretation of CAM 144 (Fig. 4D) shows the northward continuation of the Hobby High to be cut by three high angle faults with an eastward apparent dip, again offsetting the H-reflector. One of these faults, or possibly the set, may be the northward continuation of the steeply dipping fault observed at the Hobby High. No high-angle faults are identified east of the Hobby High, although several northwest dipping reflectors are identified with a steeper dip than the H-reflector such that, in places, they appear to cross-cut it. However, these latter northwest-dipping reflectors are not associated with any clear offset in the H-reflector and therefore we cannot infer their relative age.

Finally, by analogy with the E-W oriented profiles, the wedge shaped basement blocks identified in CAM 160 may indicate a component of extension oriented in the north-south direction along this region of the West Iberia margin. Similar geometries on nearby, parallel profiles have been interpreted by Clark *et al.* (2007) as evidence of southward transport of continental blocks in a mass wasting event. In the absence of further evidence, this profile merely provides an example of the complexity of a region that is inherently very three-dimensional in character.

7 CONCLUSIONS

(1) A low-angle intracrustal reflector called the H-reflector is identified on a series of intersecting depth migrated seismic reflection profiles in the vicinity of the basement high at ODP Site 900 (Hobby High) that defines the base of a series of faulted and rotated blocks of continental crust.

(2) The H-reflector forms a surface that extends laterally over a region at least 200 km^2 and dips down at a low angle (<25°) to the north, toward Galicia Bank, and at an even lower angle (<20°) down to the west in east-west profiles.

(3) Our data suggest that the detachment fault associated with the H-reflector probably extends more than 15 km east of the Hobby High.

(4) Blocks of continental crust form the basement highs adjacent to the southern flank of Galicia Bank at the northern end of our study area, but the crust thins and disappears to the south.

(5) The orientation of the blocks of continental crust above the H-reflector indicates that crustal extension was primarily in an east-west direction, but with a possible small north-south component.

ACKNOWLEDGEMENTS

Data acquisition was funded by the UK Natural Environment Research Council (NERC), and Dean was funded by a NERC research studentship for part of this work. Depth focusing error migration velocity analysis was conducted during a visit by Dean to GEOMAR, Kiel funded by the EU Access to Large Scale Facilities program. We would like to thank Dirk Kläschen for all his help, and Roger Scrutton, Nicky White, Rose Edwards, Simon Topping and Donna Shillington for constructive comments on earlier versions of the manuscript.

REFERENCES

Abers, G. A., Mutter, C. Z. & Fang, J., 1997. Shallow dips of normal faults during rapid extension: earthquakes in the Woodlark-D'Entrecasteaux rift system, Papua New Guinea, *J. Geophys. Res.*, **102**, 15301–15317.

Benes, V., Scott, S. D. & Binns, R. A., 1994. Tectonics of rift propagation into a continental margin: Western Woodlark Basin, Papua New Guinea, *J. Geophys. Res.*, **99**, 4439–4455.

Beslier, M.-O., Ask, M. & Boillot, G., 1993. Ocean-continent boundary in the Iberia Abyssal Plain from multichannel seismic data, *Tectonophysics*, **218**, 383–393.

Boillot, G., Girardeau, J. & Kornprobst, J., 1988. Rifting of the Galicia margin: crustal thinning and emplacement of mantle rocks on the seafloor, *Proc. Ocean Drill. Program, Sci. Results*, **103**, 741–756.

British Oceanographic Data Centre, 1997. *GEBCO Digital Atlas* compiled by Fisher, R. L.

Buck, W. R., 1988. Flexural rotation of normal faults, *Tectonics*, **7**, 959–973.

Chalmers, J. A., 1991. New evidence on the structure of the Labrador Sea/Greenland continental margin, *J. Geol. Soc. London*, **148**, 899–908.

De Charpal, O., Guennoc, P., Mantadert, L. & Roberts, D. G., 1978. Rifting, crustal attenuation and subsidence in the Bay of Biscay, *Nature*, **275**, 706–711.

Chian, D., Louden, K. E., Minshull, T. A. & Whitmarsh, R. B., 1999. Deep structure of the ocean–continent transition in the southern Iberia Abyssal Plain from seismic

refraction profiles: Ocean Drilling Program (Legs 149 and 173) transect, *J. Geophys. Res.*, **104**, 7443–7462.

Clark, S. A., Sawyer, D. S., Austin, J. A. Jr., Christeson, G. L. & Nakamura, Y., 2007. Characterizing the Galicia Bank-Southern Iberia Abyssal Plain rifted margin segment boundary using multichannel seismic and ocean bottom seismometer data, *J. Geophys. Res.*, **112**, 3408, doi:10.1029/2006JB004581.

Cochran, J. R. & Martinez, F., 1988. Evidence from the northern Red Sea on the transition from continental to oceanic rifting, *Tectonophysics*, **153**, 25–53.

Dean, S. M., Minshull, T. A., Whitmarsh, R. B. & Louden, K. E., 2000. Deep structure of the ocean-continent transition in the southern Iberia Abyssal Plain from seismic refraction profiles: The IAM-9 transect at 40°20'N, *J. Geophys. Res.*, **105**, 5859–5885.

Discovery 215 Working Group (Minshull, T. A., Dean, S. M., Whitmarsh, R. B., Russell, S. M., Louden, K.E. & Chian, D.), 1998. Deep structure in the vicinity of the ocean-continent transition zone under the southern Iberia Abyssal Plain, *Geology*, **26**, 743–746.

Henning, A. T., Sawyer, D. S. & Templeton, D. S., 2004. Exhumed upper mantle within the ocean-continent transition of the northern West Iberia margin: Evidence from prestack depth migration and total tectonic subsidence analyses, *J. Geophys. Res.*, **109**, 5103, doi:10.1029/2003JB002526.

Hoffmann, H.-J. & Reston, T. J., 1992. Nature of the S reflector beneath the Galicia Banks rifted margin: preliminary results from prestack depth migration, *Geology*, **20**, 1091–1094.

Jeannot, J. P., Faye, J. P. & Denelle, E., 1986. Prestack migration velocities from depth focusing analysis, *56th Ann. Internat. Mtg., Soc. Expl. Geophys., Extended Abstracts*, 438–440.

Judson, D. R., Lin, J., Schultz, P. S. & Sherwood, J. W. C., 1980. Depth migration after stack, *Geophysics*, **45**, 361–375.

Keen, C. E., Boutilier, R., de Voogd, B., Mudford, B. & Enachescu, M. E., 1987. Crustal geometry and extensional models for the Grand Banks, Eastern Canada: constraints from deep seismic reflection data, in *Sedimentary Basins and Basin-Forming Mechanisms*, Canadian Society of Petroleum Geologists, Memoir 12, pp. 101–115, eds Beaumont, C. & Tankard, A. J.

Krawczyk, C. M., Reston, T. J., Beslier, M.-O. & Boillot, G., 1996. Evidence for detachment tectonics on the Iberia Abyssal Plain rifted margin, *Proc. Ocean Drill. Program, Sci. Results,* **149**, 603–615.

Lavier, L. L. & Manatschal, G., 2006. A mechanism to thin the continental lithosphere at magma-poor margins, *Nature*, **440**, 324–328.

Le Pichon, X. & Barbier, F., 1987. Passive margin formation by low-angle faulting within the upper crust: the Northern Bay of Biscay margin, *Tectonics*, **6**, 133–150.

Lister, G. S. & Davis, G. A., 1989. The origin of metamorphic core complexes and detachment faults formed during Tertiary continental extension in the northern Colorado River region, U.S.A., *J. Struct. Geol.*, **11**, 65–94.

MacKay, S. & Abma, R., 1992. Imaging and velocity estimation with depth-focusing analysis, *Geophysics*, **57**, 1608–1622.

Manatschal, G., Froitzheim, N., Rubenach, M. & Turrin, B. D., 2001. The role of detachment faulting in the formation of an ocean-continent transition: insights from the Iberia Abyssal Plain, in *Non-Volcanic Rifting of Continental Margins: A Comparison of Evidence from Land and Sea*, Geological Society Special Publications No. 187, eds Wilson, R. C. L., Whitmarsh, R. B., Taylor, B.. & Froitzheim, N., 405–428.

Manatschal, G., 2004. New models for evolution of magma-poor rifted margins based on a review of data and concepts from West Iberia and the Alps, *Int. J. Earth Sci.*, **93**, 432–466.

ODP Leg 173 Shipboard Scientific Party, 1998. Drilling reveals transition from continental breakup to early magmatic crust, *EOS Trans. AGU*, **79**, 173–181.

Ogg, J. G., 1988. Early Cretaceous and Tithonian magnetostratigraphy of the Galicia margin, *Proc. Ocean Drill. Program, Sci. Results*, **103**, 659–682.

Pérez-Gussinyé, M., Ranero C. R. & Reston, T. J., 2003. Mechanisms of extension at nonvolcanic margins: Evidence from the Galicia interior basin, west of Iberia, *J. Geophys. Res.*, **108**, 2245, doi:10.1029/2001JB000901.

Péron-Pinvidic, G., Manatschal, G, Minshull, T. A. & Sawyer, D., 2007, The tectono-sedimentary and morpho-tectonic evolution recorded in the deep Iberia-Newfoundland margins: Evidence for a complex break-up history, *Tectonics*, **26**, 2011, doi:10.1029/2006TC001970.

Péron-Pinvidic, G., G. Manatschal, Dean, S. M. & Minshull, T. A., 2008, Compressional structures on the West Iberia rifted margin: what controls their

distribution? In: *The Nature and Origin of Compression in Passive Margins*, *Geol. Soc. London Special Publication*, London, Geological Society, in press.

Pickup, S. L. B., Whitmarsh, R. B., Fowler, C. M. R. & Reston, T. J., 1996. Insight into the nature of the ocean-continent transition off West Iberia from a deep multichannel seismic reflection profile, *Geology*, **24**, 1079–1082.

Pinheiro, L. M., Whitmarsh, R. B. & Miles, P. R., 1992. The ocean-continent boundary off the western continental margin of Iberia - II. Crustal structure in the Tagus Abyssal Plain, *Geophys. J. Int.*, **109**, 106–124.

Pinheiro, L. M., Wilson, R. C. L., Pena dos Reis, R., Whitmarsh, R. B. & Ribeiro, A., 1996. The western Iberia margin: a geophysical and geological overview, *Proc. Ocean Drill. Program, Sci. Results*, **149**, 3–23.

Ranero, C. R. & Reston, T. J., 1999. Detachment faulting at ocean core complexes, *Geology*, **27**, 983–986.

Reitbrock, A., Tiberi, C., Scherbaum, F. & Lyon-Caen, H., 1996. Seismic slip on a low angle normal fault in the Gulf of Corinth: evidence from high-resolution cluster analysis of microearthquakes, *Geophys. Res. Lett.*, **23**, 1817–1820.

Reston, T. J., Krawczyk, C. M. & Hoffmann, H.-J, 1995. Detachment tectonics during Atlantic rifting: analysis and interpretation of the S reflector, the west Galicia margin, in *The Tectonics, Sedimentation and Palaeoceanography of the North Atlantic Region*, Geological Society Special Publications No. 90, eds Scrutton, R. A., Stoker M. S., Shimmield, G. B. & Tudhope, A. W., 93–109.

Reston, T. J., Krawczyk, C. M. & Klaeschen, D., 1996. The S reflector west of Galicia (Spain): evidence from prestack depth migration for detachment faulting during continental breakup, *J. Geophys. Res.*, **101**, 8075–8091.

Russell, S. M. & Whitmarsh, R. B., 2003. Magmatism at the west Iberia non-volcanic rifted continental margin: evidence from analyses of magnetic anomalies, *Geophys. J. Int.*, **154**, 706–730.

Sibuet, J.-C., Mazé, J.-P., Amortila, P. & Le Pichon, X., 1987. Physiography and structure of the western Iberian continental margin off Galicia, from sea beam and seismic data, *Proc. Ocean Drill. Program, Init. Repts.*, **103**, 77–97.

Srivastava, S. P. & Verhoef, J., 1992. Evolution of Mesozoic sedimentary basins around the North Central Atlantic: a preliminary plate kinematic solution, in *Basins on the Atlantic Seaboard: Petroleum Geology, Sedimentology and Basin Evolution*, Geological Society Special Publications No. 62, editor Parnell, J, 397–420.

Tucholke, B.E. & Lin. J., 1994. A geological model for the structure of ridge segments in slow spreading ocean crust, *J. Geophys. Res.*, **99**, 11937–11958.

Versteeg, R. J., 1993. Sensitivity of prestack depth migration to the velocity model, *Geophysics*, **58**, 873–882.

Wernicke, B., 1981. Low-angle normal faults in the Basin and Range Province: nappe tectonics in an extending orogen, *Nature*, **291**, 645–647.

Whitmarsh, R. B. & Miles, P. R., 1995. Models of the development of the West Iberia rifted continental margin at 40°30'N deduced from surface and deep-tow magnetic anomalies, *J. Geophys. Res.*, **100**, 3789–3806.

Whitmarsh, R. B., Beslier, M.-O., Wallace, P. J., *et al*., 1998. *Proc. Ocean Drill. Program, Init. Repts.*, **173**.

Whitmarsh, R. B., Dean, S. M., Minshull, T. A. & Tompkins, M., 2000. Tectonic implications of exposure of lower continental crust beneath the Iberia Abyssal Plain, Northeast Atlantic Ocean: Geophysical evidence, *Tectonics*, **19**, 919–942.

Whitmarsh, R. B., Manatschal, G. & Minshull, T. A., 2001. Evolution of magma-poor continental margins from rifting to seafloor spreading, *Nature*, **413**, 150–154.

Wilson, R. C. L., Sawyer, D. S., Whitmarsh, R. B., Zerong, J. & Carbonell, J., 1996. Seismic stratigraphy and tectonic history of the Iberia Abyssal Plain, *Proc. Ocean Drill. Program, Sci. Results*, **149**, 617–633.

Yilmaz, O., 1987. Seismic Data Processing, *Investigations in Geophysics 2, Society of Exploration Geophysicists*, Tulsa, Oklahoma.

FIGURE CAPTIONS

Figure 1. Bathymetric map for the West Iberia Atlantic margin contoured in 500-m intervals (British Oceanographic Data Centre 1997). Dashed black lines locate pre-existing MCS profiles (Fig. 2). Solid grey lines identify the peridotite ridge segments R1–R4 interpreted from seismic reflection profiles (Beslier *et al*. 1993; Pickup *et al*. 1996). Dashed grey lines mark the J magnetic anomaly (Pinheiro *et al*. 1992). The inset map expands the area around the ODP drilling transect. Thin lines identify the Discovery DY215 survey track; dashed lines identify Lusigal 12 and IAM-9 seismic profiles; dotted lines identify other seismic reflection profiles; bold lines mark sections from multichannel seismic profiles CAM 134, CAM 144, CAM 146, CAM 159 and CAM 160 presented in this paper; grey area identifies the extent of continental crust along the seismic profiles as defined by Chian *et al*. (1999), west of Site 900, and this paper, east of Site 900. Circles locate Ocean Drilling Program sites from Legs 149 and 173.

Figure 2. Key multichannel seismic profiles, located on the West Iberia Atlantic margin (Fig. 1), that span the ocean-continent transition. The locations of ODP drill sites are labelled at the top of each section and enclosed by brackets where they have been projected onto the profile. R2–R4 are segments of the peridotite ridge identified by Pickup *et al*. (1996). A transition zone is identified for each profile, following the definition of Pickup *et al*. (1996), lying between the peridotite ridge and the oceanward extent of continuous continental crust. (A) IAM-11 time migrated with interpretation after Reston *et al*. (1995) and Reston *et al*. (1996) of the S-reflector (S) west of ODP Site 639, Pérez-Gussinyé *et al*. (2003) east of Site 639. (B) Lusigal 12 time migrated and interpretation of the H-reflector (H) after Krawczyk *et al*. (1996) with the ODP Site

1069 continental allochthon after ODP Leg 173 Shipboard Scientific Party (1998); Sites 1065 and 1069 lie ~5 km north of this profile. (C) IAM-9 time migrated (Pickup *et al*. 1996). Major sub-basement reflections identified include a discontinuous Moho (M) and a pair of landward dipping events L1 and L2.

Figure 3. (A) CAM 146 migration velocity model, contoured in km s^{-1}, derived from iterative depth focusing analysis and wide-angle seismic velocities (see text for details); triangles at the top of the section locate intersections with other CAM profiles. (B) Depth migrated image of CAM 146. (C) Interpretation of the basement structure. This profile has a very similar appearance to the Lusigal 12 profile, which lies parallel to CAM 146, but ~5 km to the north; the basement high beneath CDP 2450 is the southward continuation of the Hobby High. Beneath CDP 1400–2250 fault bounded basement blocks are capped with either a pre-rift or an early synrift sediment unit (hatched areas) and are draped by synrift units (dotted areas), similar to the interpretation of Krawczyk *et al*. (1996). The H-reflector (H) is clearly identified below CDP 2050–2250. To the east it appears to continue beneath the basement but, to be consistent with the other MCS profiles, must rise to the basement at CDP 1850. To the west the H-reflector rises to the basement at CDP 2400 where a distinct peak is identified. To the west of the basement peak the basement shows a marked increase in reflectivity in the top 1–2 km. The vertical exaggeration is x1.5.

Figure 4. (A) CAM 144 migration velocity model, contoured in km s^{-1}, derived from iterative depth focusing analysis and wide-angle seismic velocities (see text for details); triangles at the top of the section locate intersections with other CAM profiles. (B) Depth migrated image of CAM 144; the black box indicates the portion of data enlarged in Fig. 8. (C) Interpretation of the basement structure. The H-reflector (H) is clearly

identified at the intersections with CAM 159 and CAM 160 but cannot be interpreted as a continuous reflection event in this profile. The strongest basement reflectors (dashed lines) lie beneath CDP 1950, the northward continuation of the Hobby High, and may be interpreted either as a series of low-angle, westward dipping faults shown here, or as a series of high-angle, eastward dipping faults (D). The vertical exaggeration is x1.5.

Figure 5. (A) CAM 159 migration velocity model, contoured in km s^{-1}, derived from tying velocity layers to sediment and basement reflectors at the intersection with CAM 144 and CAM 146; triangles at the top of the section locate intersections with Lusigal 12 and other CAM profiles. (B) Depth migrated image of CAM 159. (C) Interpretation of the basement structure. The H-reflector (H) is poorly imaged, probably because it is both deep and dips out of the section, and is therefore poorly migrated, but the weak reflection at ~11 km depth at CDP 1250 ties with the H-reflector identified on CAM 144 (Fig. 4). The strong sub-basement reflection observed at CDP 800–1150 lies above the H-reflector and represents one of the faults bounding a pair of basement blocks when tied with the other MCS profiles; the strong reflector must merge with the H-reflector toward the southwest to form a consistent model with Lusigal 12 (Krawczyk *et al*. 1996). Two possible interpretations for the H-reflector are given (dashed lines). Close to the intersection with CAM 146 the H-reflector is interpreted to truncate against a dipping reflector with a steep apparent dip down to the northeast, similar to the interpretation of CAM 146 (Fig. 3C), although the relationship is not well constrained in this profile. The vertical exaggeration is x1.5.

Figure 6. (A) CAM 160 migration velocity model, contoured in km s^{-1}, derived from iterative depth focusing analysis and wide-angle seismic velocities (see text for details); triangles at the top of the section locate intersections with Lusigal 12 and other CAM

profiles. (B) Depth migrated image of CAM 160. (C) Interpretation of the basement structure. The H-reflector (H) is clearly identified dipping down toward the north (Galicia Bank). To be consistent with interpretations of Lusigal 12 (e.g., Manatschal 2004) the H-reflector must rise to the basement at CDP 600. Between CDP 600–1000 the basement is cut into a number of small wedges, overlain with a synrift sediment unit (dotted area), by northward dipping faults that suggest a N–S oriented component of extension. The detail of this interpretation at the intersection with CAM 146, including the deep reflection marked with a dashed line between CDP 400–850, is shown in Fig. 10. The vertical exaggeration is x1.5.

Figure 7. Velocity uncertainty within a model layer versus two-way travel-time through the layer for curves representing various estimates of the uncertainty in the depth of the base of the layer. The shaded region covers the range of layer travel-time thicknesses used in migration velocity models for the DY215 MCS data; the estimated velocity uncertainty in a single focusing velocity analysis, assuming a depth uncertainty of 0.04 km (bold line) estimated from the DFA depth focusing panels (see text), is between 0.17 and 0.4 km s^{-1}.

Figure 8. (A) Detail from the depth migrated section of CAM 144 (Fig. 4). The reflector used to define the top of sediment Unit 6C, indicated by the arrow, has a vertical offset at CDP 1580 where the high amplitude reflection from the top of Unit 6 ends at 6.5 km depth. (B) The velocity layers used to migrate the data in (A). (C) The offset in the Unit 6C reflector is mostly removed by the introduction of a high velocity layer into the migration velocity model for the overlying sediments (D).

Figure 9. Unmigrated stacked sections showing the tie between reflection events at the point of intersection between (A) CAM 159 and CAM 144; (B) CAM 160 and CAM

144; (C) CAM 159 and Lusigal 12; (D) CAM 160 and CAM 146. Arrows identify the H-reflector with a tick marking the two-way travel time where the profiles intersect.

Figure 10. Detail from the intersection between CAM 160 and CAM 146 showing the H-reflector (solid line), fault bounded basement blocks above the H-reflector (dotted lines), and reflectors below the H-reflector (dashed lines).

Figure 11. The interpretation of the basement and H-reflector (bold line), in depth, determined from migrated seismic reflection profiles. Dashed lines indicate other strong sub-basement reflectors that lie structurally below the H-reflector. Dotted lines indicate reflectors that either intersect or form a part of the basement. Faulted blocks of continental crust are coloured light grey; dark grey regions are either lower continental crust or mantle. ODP Leg 149 and 173 sites are numbered. The interpretation of Lusigal 12 is after Krawczyk *et al*. (1996), ODP Leg 173 Shipboard Scientific Party (1998) and Manatschal (2004). The horizontal scale is in (km); the vertical exaggeration is x1. The inset shows an alternate interpretation for the H-reflector, beneath all the faulted blocks of continental crust identified on CAM 146 and CAM 160.

Figure 12. Time migrated sections showing the relationship between the basement high at the west end of CAM 144 and the small block of continental crust, sampled at ODP Site 1069 (CAM 134; Whitmarsh *et al*. 1998), and observed on Lusigal 12 in apparent isolation oceanward of the Hobby High.

TABLES

Table 1. Processing steps applied to the DY215 MCS field data to provide a final depth section. Times quoted for predictive deconvolution cover only the filter design window and, for the bandpass filter, do not include the 500 ms ramp time. The processing step 'Velocity analysis' is described in detail in the text.

Processing step	Parameters
Geometry installation	
Desample	4 ms – 8 ms
Static shift	-50 ms
Amplitude recovery	T^2
Predictive deconvolution	200 ms operator / 80 ms gap seafloor+200 ms to basement+1000 ms
Bandpass filter	3-5-20-60 Hz : 0 to basement-500 ms 3-5-20-24 Hz : basement+500 to 16000 ms
Velocity analysis	Iterative depth focusing error migration velocity analysis (DFA)
Migration	Kirchhoff prestack depth migration
Datum correction	+20 m

Table 2. Seismic velocities determined by iterative migration velocity analysis on lines CAM 144, CAM 146 and CAM 160 for the sedimentary Units identified by Wilson *et al*. (1996) in the vicinity of the ODP Leg 149 drill sites.

Sedimentary Unit	Approximate velocity (km s^{-1})	Typical thickness (km)
Units 1 & 2	1.7	0.15
Unit 3	1.7–1.85	0.4
Unit 4	2.4–3.0	0.8
Unit 5	3.2	0.15
Unit 6A & 6B	3.2	<0.6
Unit 6C	3.5	<0.6
Pre-rift/Synrift	3.8	<1.5

FIGURES

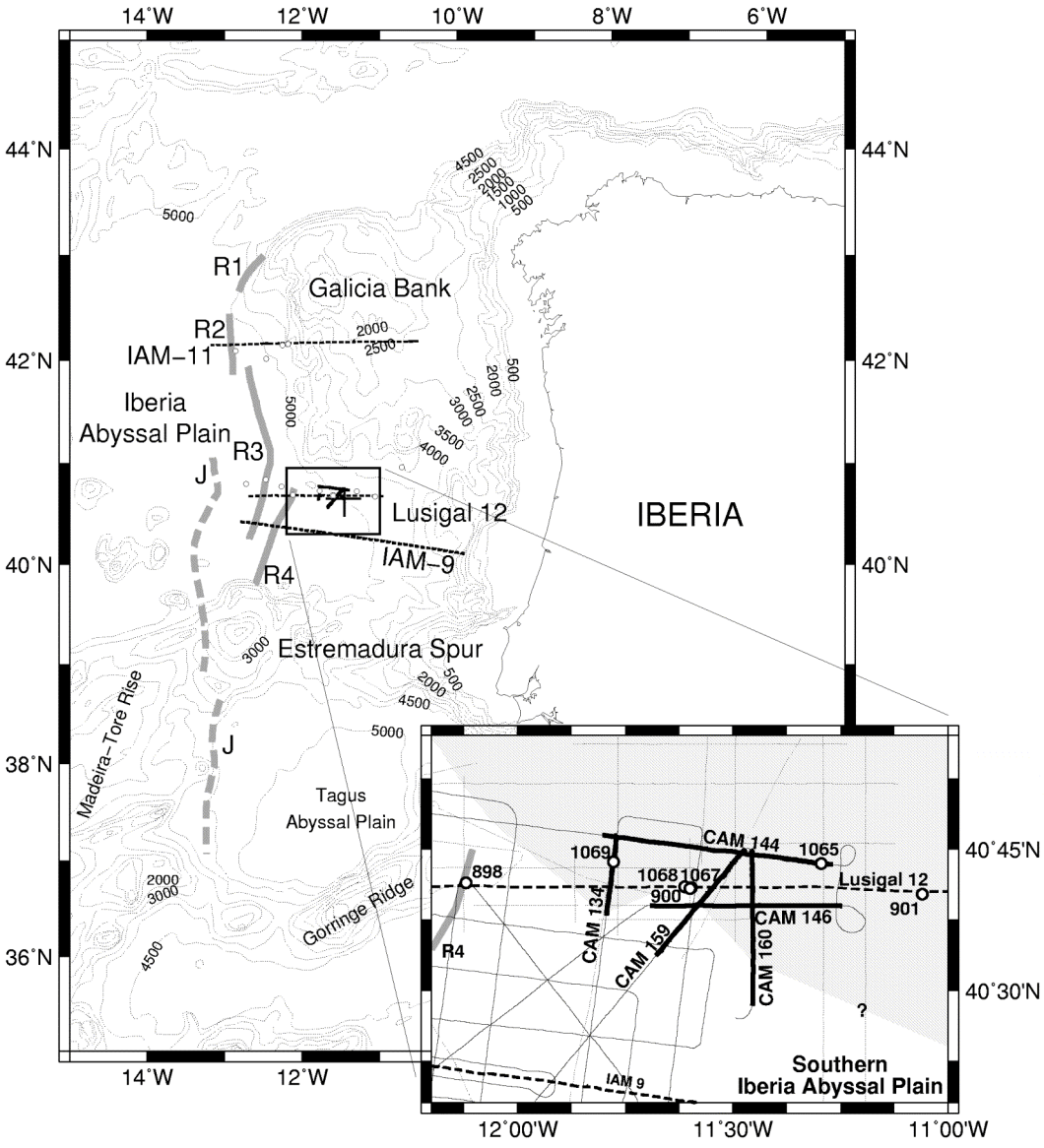

Figure 1

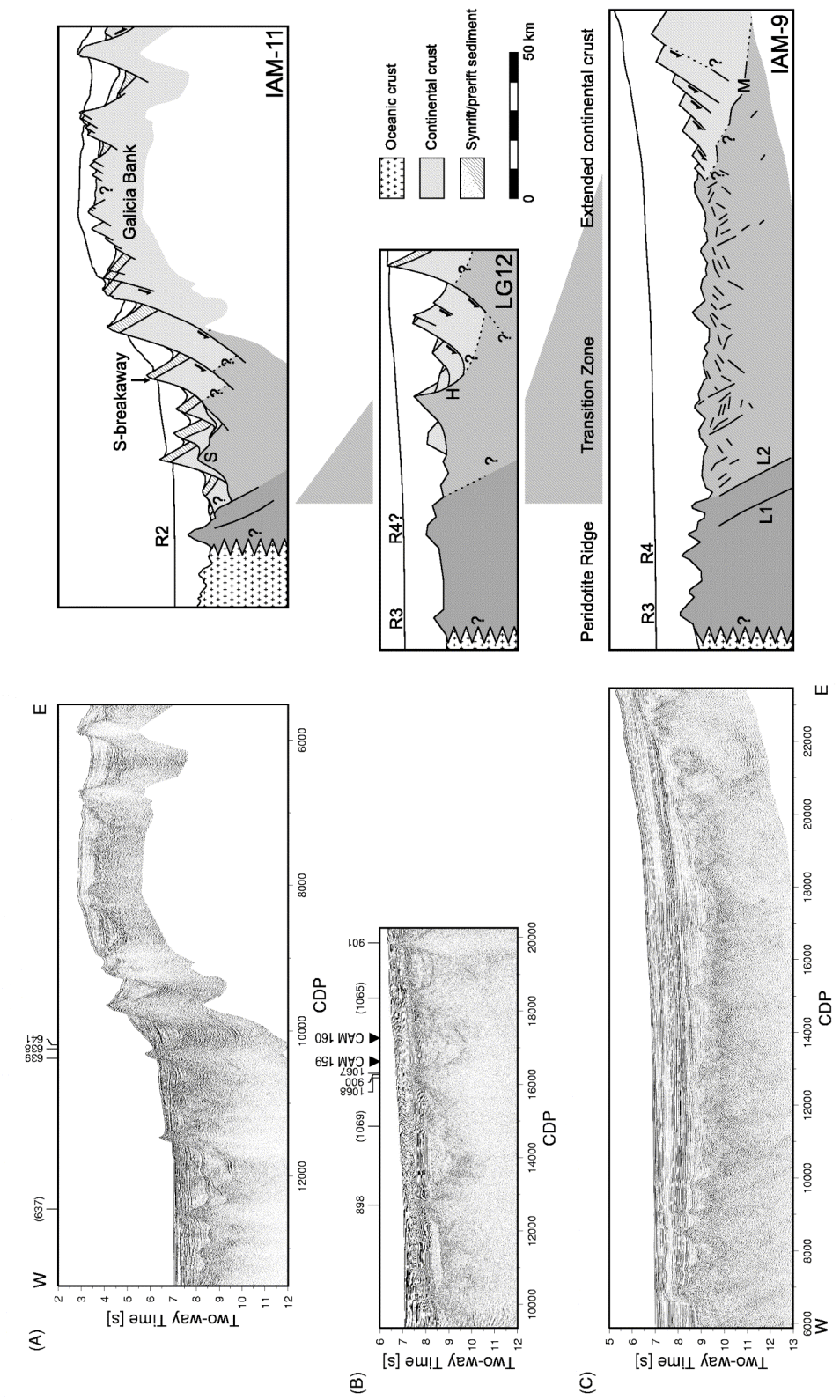
IAM-11
Galicia Bank
S-breakaway
S
R2
LG12
R3
R4?
H
IAM-9
Peridotite Ridge
Transition Zone
Extended continental crust
R3
R4
L1
L2
M
Oceanic crust
Continental crust
Synrift/prerift sediment
0
50 km
(A)
W
E
(637)
639
641
642
Two-way Time [s]
CDP
(B)
898
(1069)
1068
900
1067
CAM 159
CAM 160
(1065)
901
Two-way Time [s]
CDP
(C)
W
E
Two-way Time [s]
CDP

Figure 2

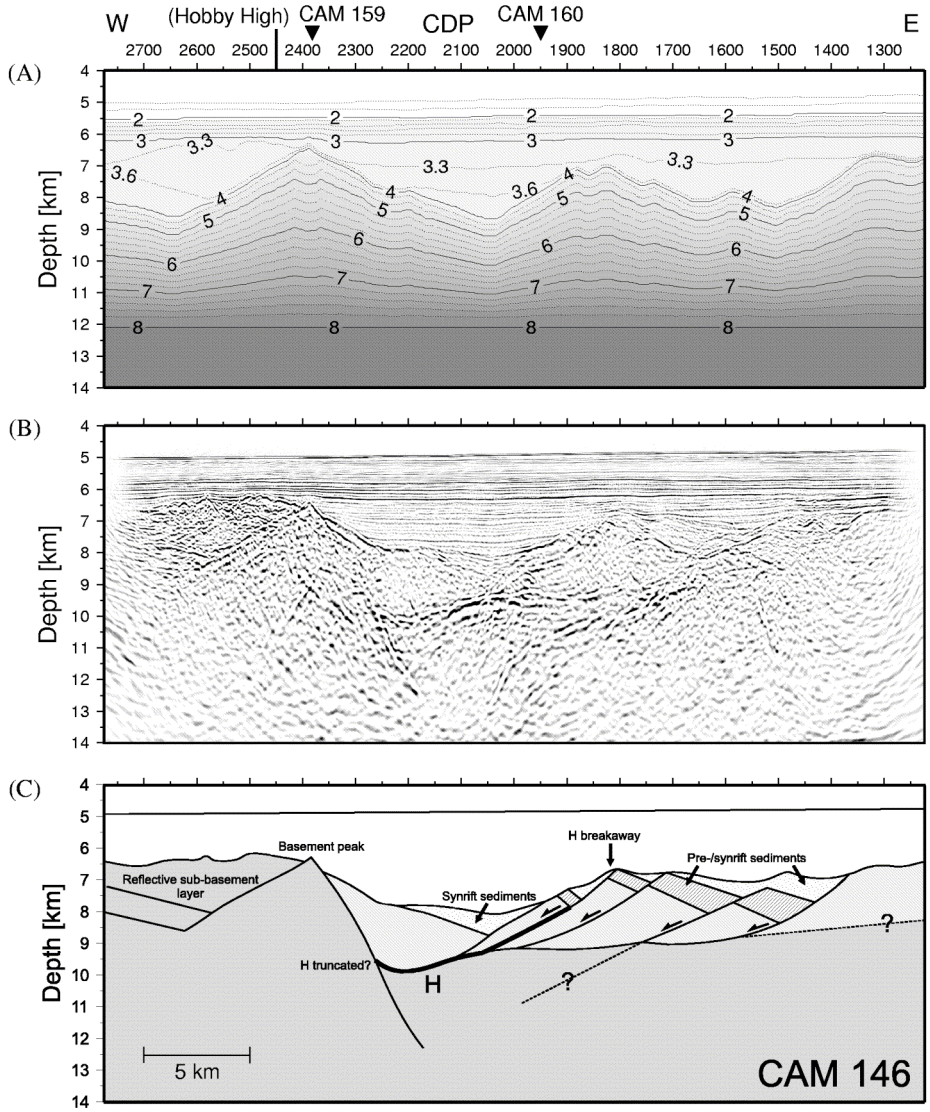
W
(Hobby High)
CAM 159
CDP
CAM 160
E
2700 2600 2500 2400 2300 2200 2100 2000 1900 1800 1700 1600 1500 1400 1300
(A)
(B)
(C)
Depth [km]
Basement peak
Reflective sub-basement layer
Synrift sediments
H breakaway
Pre-/synrift sediments
H truncated?
H
5 km
CAM 146

Figure 3

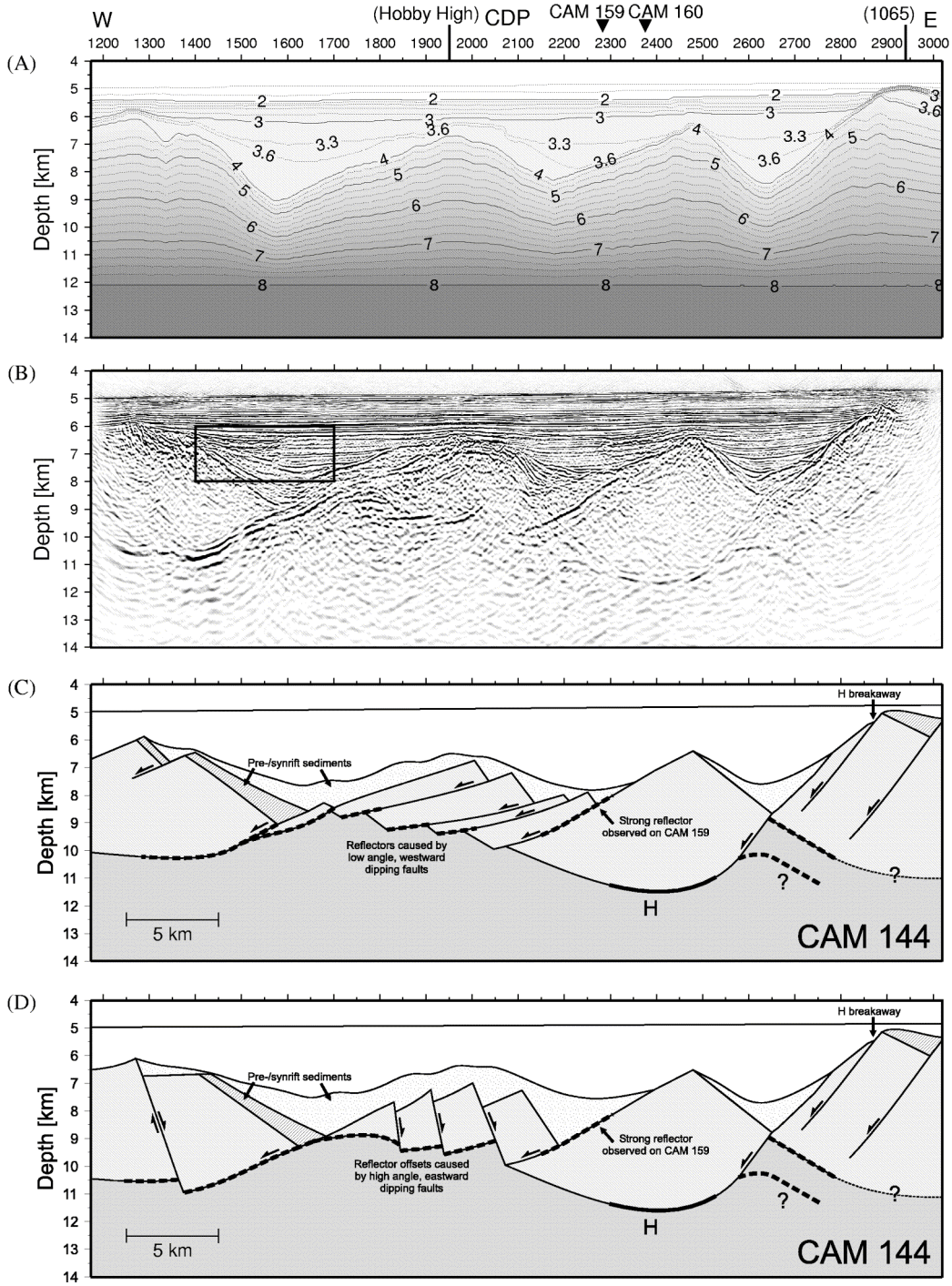
W
(Hobby High)
CDP
CAM 159
CAM 160
(1065)
E
(A)
(B)
(C)
(D)
Depth [km]
H breakaway
Pre-/synrift sediments
Strong reflector observed on CAM 159
Reflectors caused by low angle, westward dipping faults
Reflector offsets caused by high angle, eastward dipping faults
H
5 km
CAM 144

Figure 4

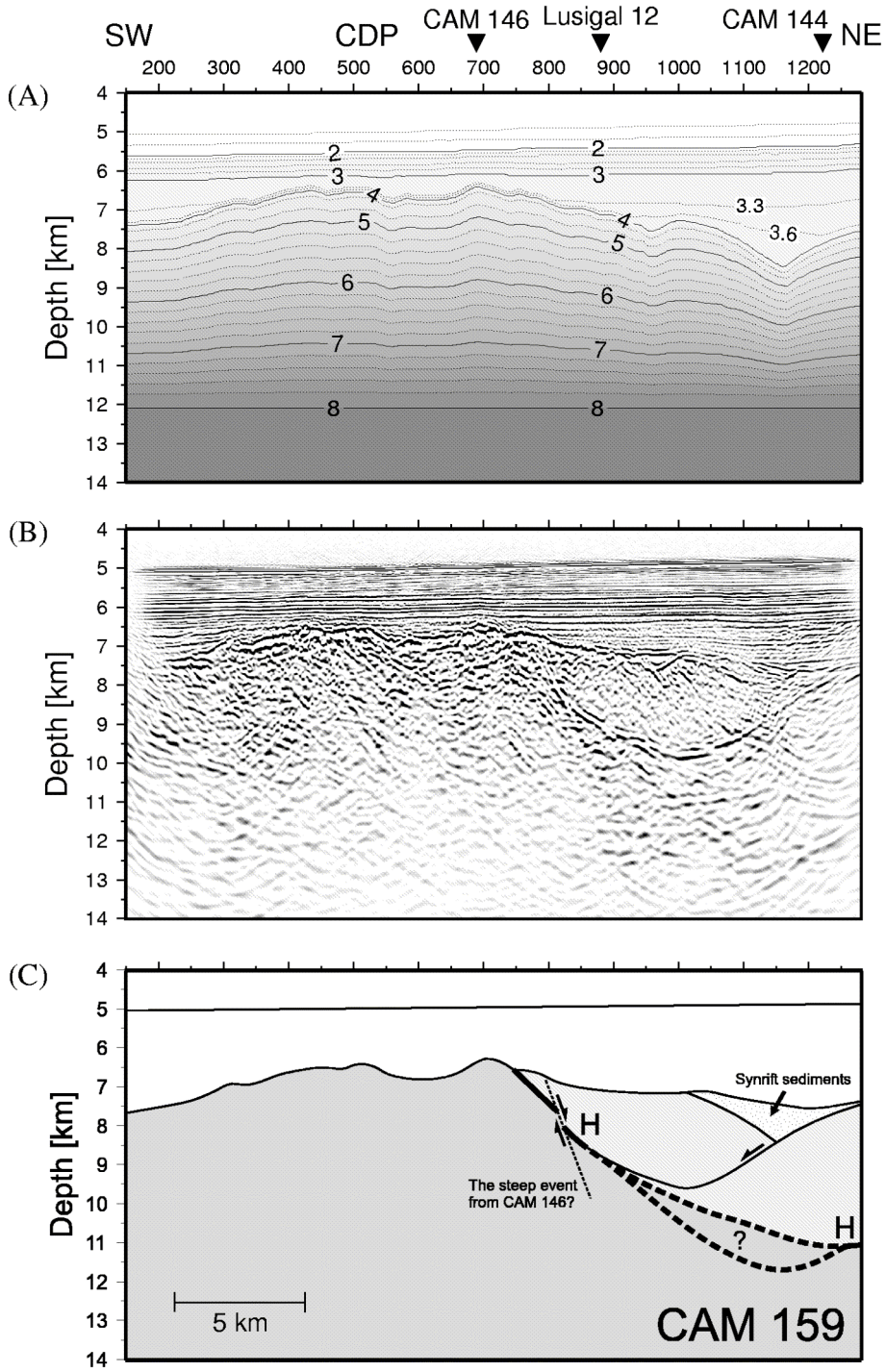
SW
CDP
CAM 146
Lusigal 12
CAM 144
NE
200
300
400
500
600
700
800
900
1000
1100
1200
(A)
(B)
(C)
Depth [km]
2
3
4
5
6
7
8
3.3
3.6
Synrift sediments
H
The steep event
from CAM 146?
?
5 km
CAM 159

Figure 5

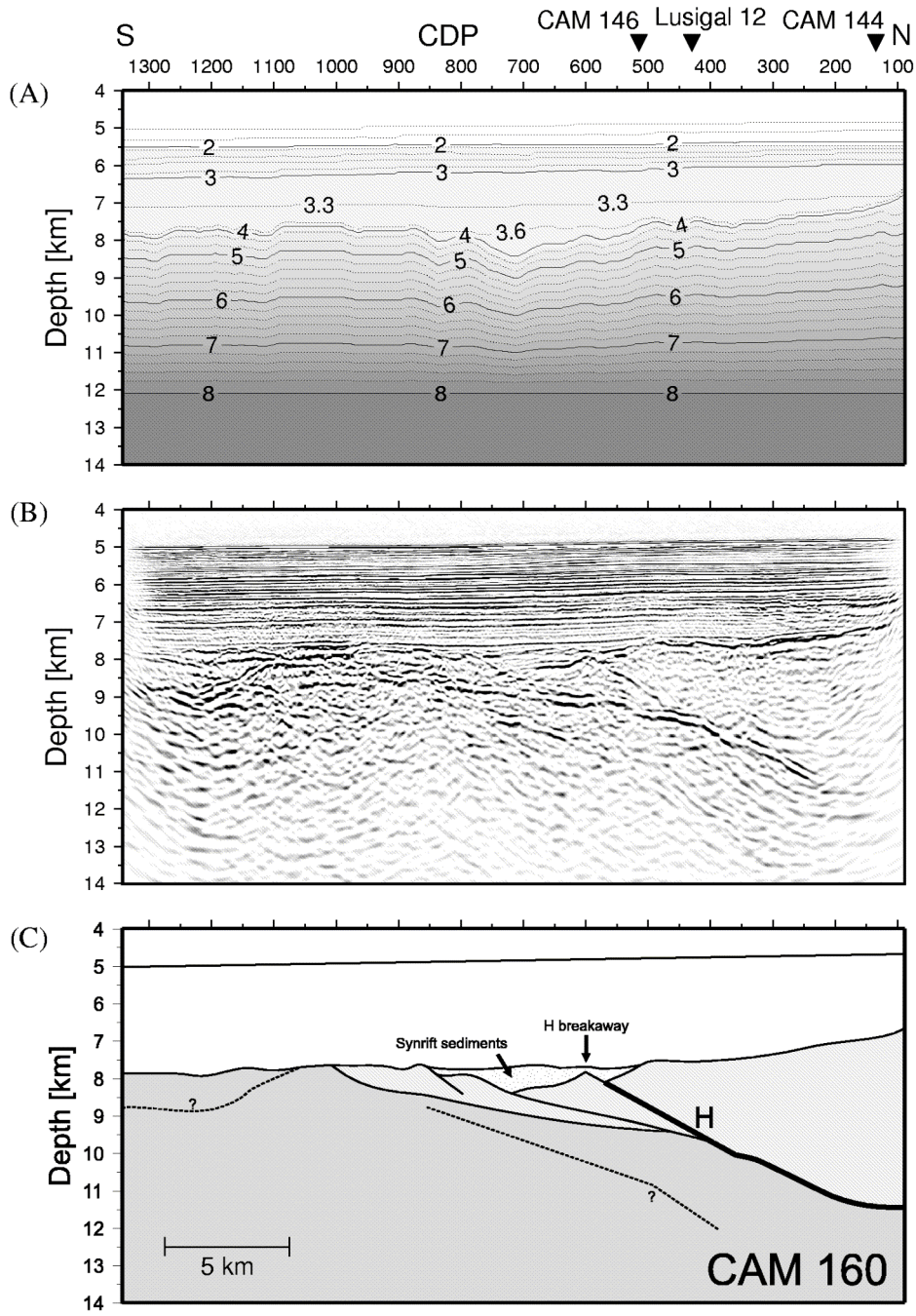
S
CDP
CAM 146
Lusigal 12
CAM 144
N
1300 1200 1100 1000 900 800 700 600 500 400 300 200 100
(A)
(B)
(C)
Depth [km]
2
3
3.3
3.6
4
5
6
7
8
Synrift sediments
H breakaway
H
?
5 km
CAM 160

Figure 6

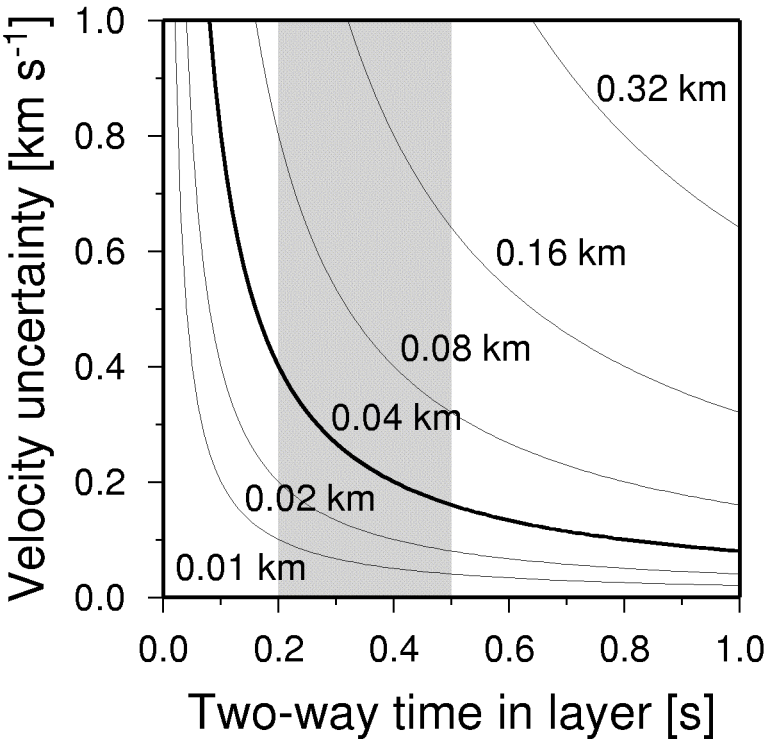
Velocity uncertainty [km s-1]
1.0
0.8
0.6
0.4
0.2
0.0
0.0
0.2
0.4
0.6
0.8
1.0
Two-way time in layer [s]
0.32 km
0.16 km
0.08 km
0.04 km
0.02 km
0.01 km

Figure 7

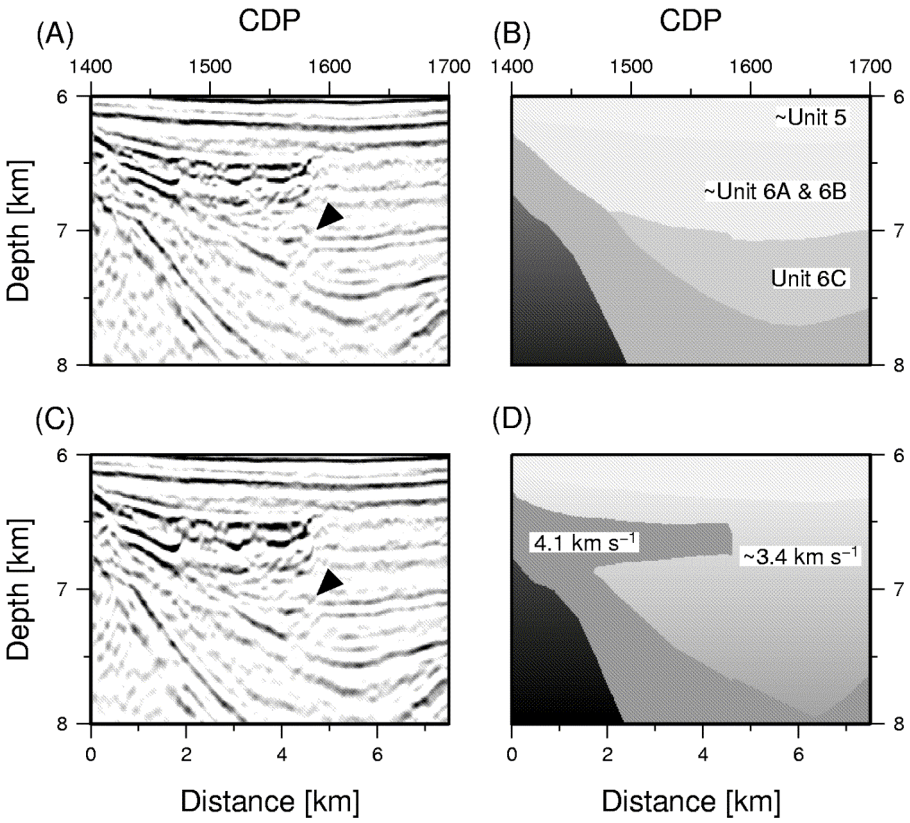
(A)
CDP
1400
1500
1600
1700
6
7
8
Depth [km]
(B)
CDP
~Unit 5
~Unit 6A & 6B
Unit 6C
(C)
(D)
4.1 km s^{-1}
~3.4 km s^{-1}
0
2
4
6
Distance [km]

Figure 8

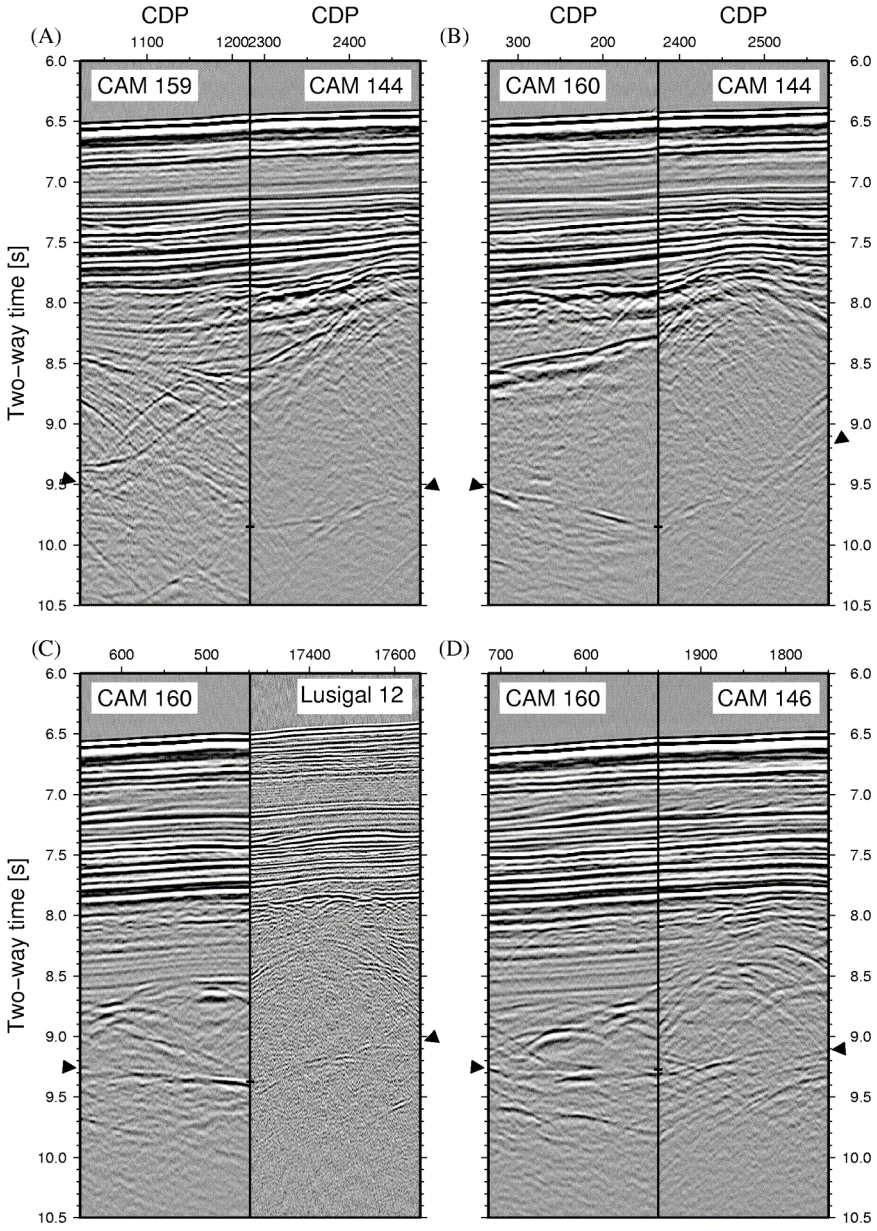
(A)
CDP
CDP
1100
1200
2300
2400
CAM 159
CAM 144
(B)
CDP
CDP
300
200
2400
2500
CAM 160
CAM 144
(C)
600
500
17400
17600
CAM 160
Lusigal 12
(D)
700
600
1900
1800
CAM 160
CAM 146
Two−way time [s]
6.0
6.5
7.0
7.5
8.0
8.5
9.0
9.5
10.0
10.5

Figure 9

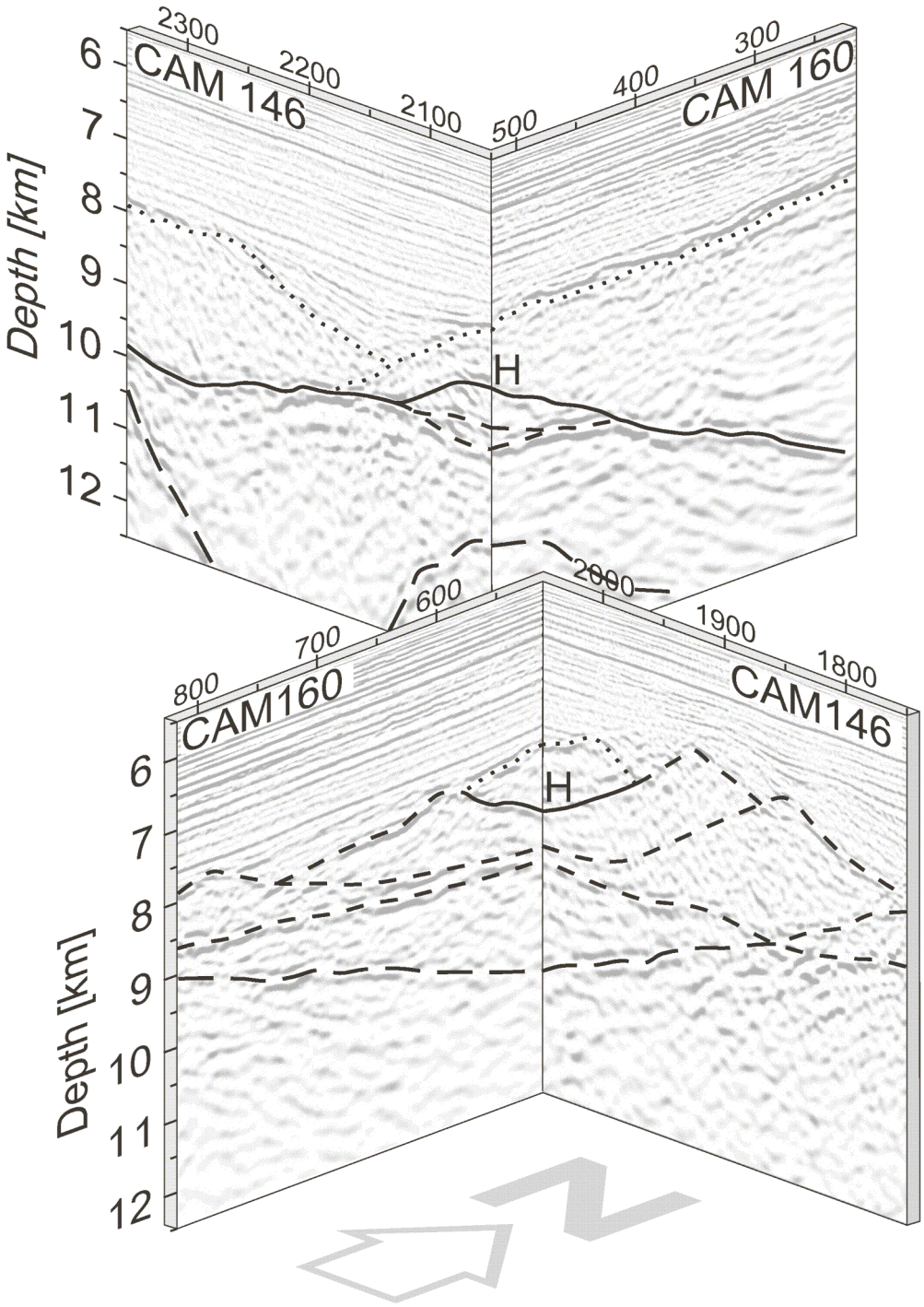
2300
2200
2100
500
400
300
CAM 146
CAM 160
Depth [km]
6
7
8
9
10
11
12
H
600
2000
700
800
1900
1800
CAM160
CAM146
H
Depth [km]
6
7
8
9
10
11
12

Figure 10

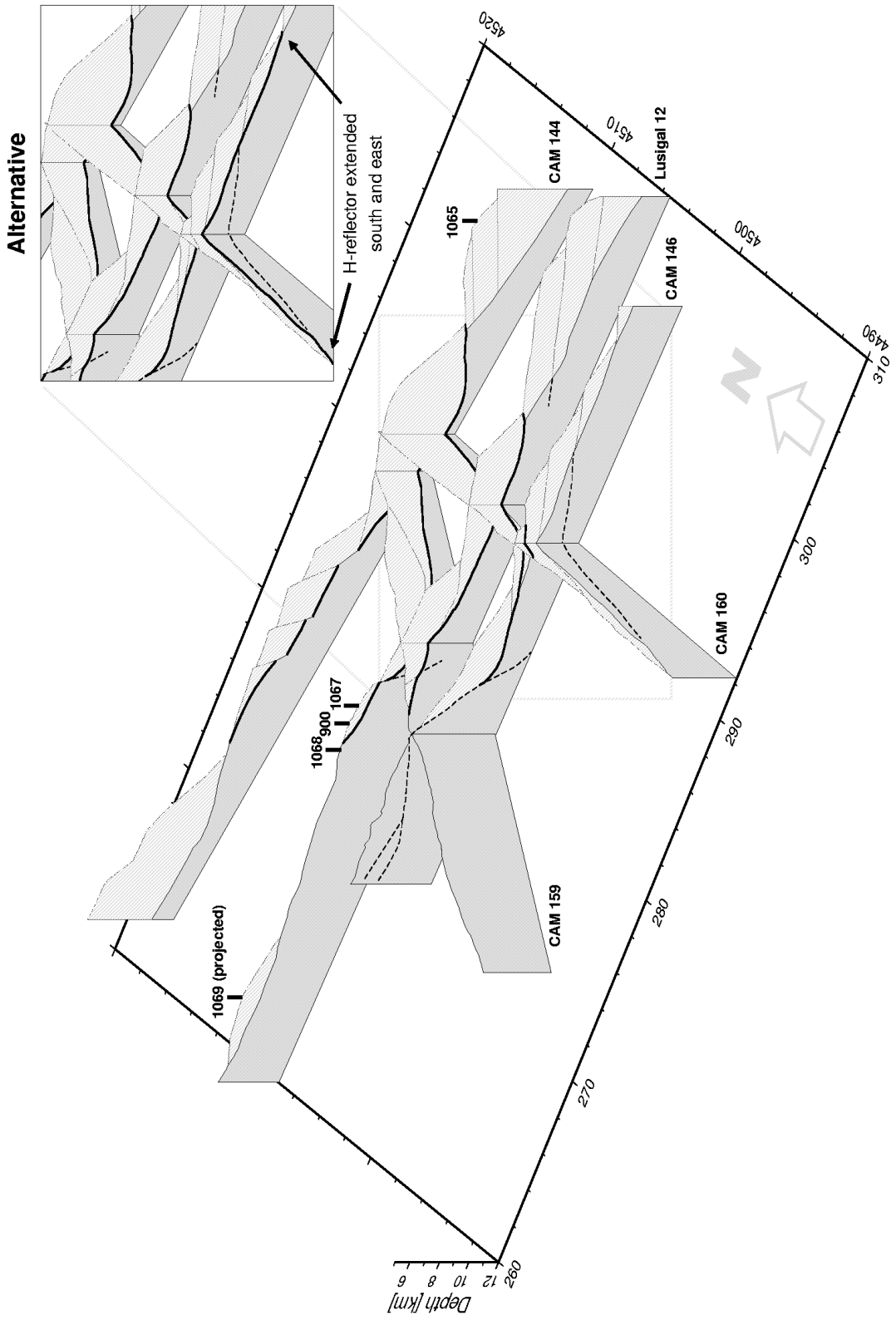
Alternative
H-reflector extended
south and east
CAM 144
Lusigal 12
CAM 146
CAM 160
CAM 159
1065
1067
900
1068
1069 (projected)
N
4520
4510
4500
4490
310
300
290
280
270
260
12
10
8
6
Depth [km]

Figure 11

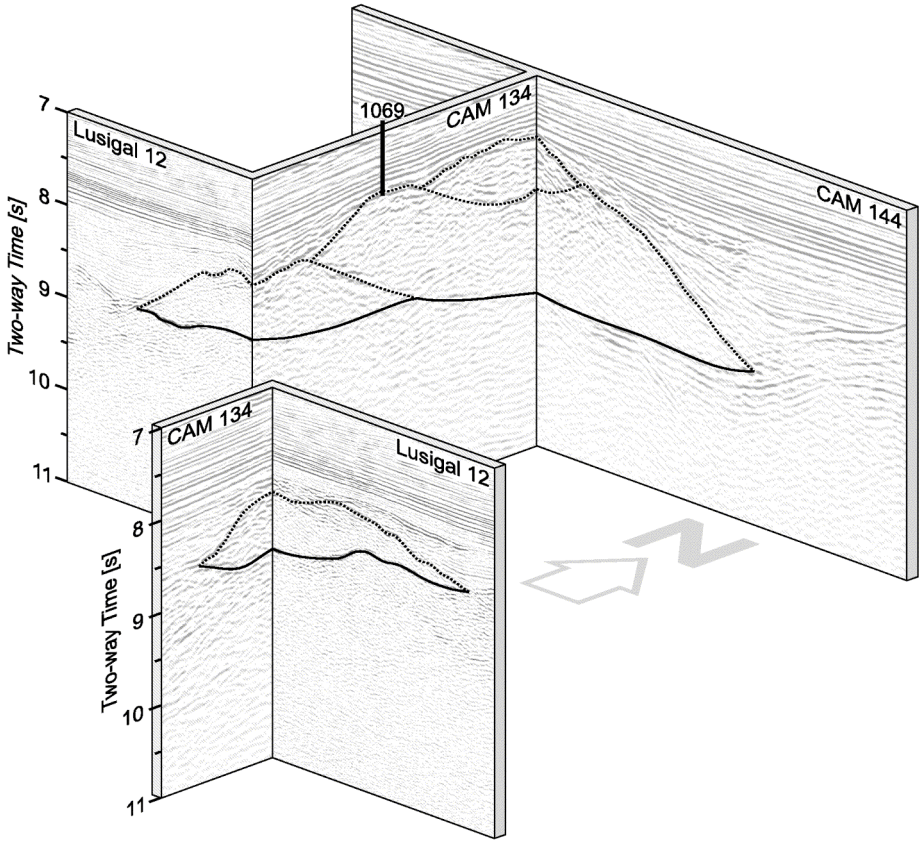
Lusigal 12
1069
CAM 134
CAM 144
Two-way Time [s]
7
8
9
10
11
CAM 134
Lusigal 12
Two-way Time [s]
7
8
9
10
11

Figure 12